Low Temperature Physics/Fizika Nizkikh Temperatur, 2012, v. 38, No. 12, pp. 1455–1463

Magnetotransport studies of SiGe-based *p*-type heterostructures: problems of the effective mass determination

I.B. Berkutov[1], V.V. Andrievskii[1], Yu.F. Komnik[1], Yu.A. Kolesnichenko[1], R.J.H. Morris[2], D.R. Leadley[2], and O.A. Mironov[2,3]

[1]*B. Verkin Institute for Low Temperature Physics and Engineering of National Academy of Sciences of Ukraine 47 Lenin Ave., Kharkov 61103, Ukraine*
E-mail: berkutov@ilt.kharkov.ua

[2]*Department of Physics, University of Warwick, Coventry CV4 7AL, UK*

[3]*International Laboratory of High Magnetic Fields and Low Temperatures 95 Gajowicka, Wroclaw 53-24, Poland*

Received June 5, 2012

The Shubnikov–de Haas oscillations method of the effective mass extraction was illustrated by the magnetotransport properties investigation of two-dimensional hole gas in $Si_{1-x}Ge_x$ (x = 0.13, 0.36, 0.95, 0.98) QWs. We have found that for certain samples our data cannot be fitted to standard theoretical curves in which the scattering of charge carriers is described by conventional Dingle factor. It is demonstrated that reasons of deviations of the experiment from the theory are as follows; (i) influence of the spin splitting on amplitude of SdH oscillations maxima; (ii) extra broadening of the Landau levels attributed to existence of inhomogeneous distribution of the carrier concentration; (iii) the influence of the concurrent existence of short and long-range scattering potentials; (iv) the population of second energy level in the quantum well. The ways to calculate the effective masses m* of holes in all cases are presented and values of m* are found for studied heterostructures.

PACS: 72.20.My Galvanomagnetic and other magnetotransport effects;
71.18.+y Fermi surface: calculations and measurements; effective mass, *g* factor;
72.20.–i Conductivity phenomena in semiconductors and insulators.

Keywords: quantum well, Shubnikov–de Haas oscillations, effective mass.

1. Introduction

One of the most attractive features resulting from band engineering in SiGe heterostructures is the enhancement that can be made to the mobility of the charge carriers. In particular, the enhancement of hole mobility is very attractive in Si/SiGe-based materials because the *p*-type device limits the performance of complementary MOS type circuits due to its intrinsically lower mobility. Among various types of SiGe heterostuctures designed to increase hole mobility μ_H, strained and high content Ge channel modulation-doped structures have provided the highest mobility at both low temperature, where $\mu_H = 120 \cdot 10^3$ cm^2/(V·s) at 2 K with a carrier density of $8.5 \cdot 10^{11}$ cm^{-2} [1], and at room temperature, where $\mu_H = 3.1 \cdot 10^3$ cm^2/(V·s) with a carrier density of $4.1 \cdot 10^{12}$ cm^{-2} [2]. This mobility increase comes primarily from the fact that the effective hole mass decreases with increasing Ge content [3].

The effective mass m^* of charge carriers is an important parameter in determining the kinetic and thermodynamic properties of the conducting system. For example, if the m^* is known, then the isotropic two-dimensional (2D) density of states for a gas of noninteracting carriers is given by $n_{2D} = m^*/(\pi\hbar^2)$. The m^* of 2D charge carriers can be measured either by quantum cyclotron resonance (CR) [4] or from Shubnikov–de Haas (SdH) oscillations [5]. Both of these methods use a magnetic field to create Landau levels within the material. Quantum cyclotron resonance directly measures the transition energy between Landau levels, but this method is limited by severe requirements concerning both the experimental conditions and the material under examination. The effective mass can also be found from the temperature dependence of the amplitude of SdH oscillations. This method introduces some averaging, but typically works at lower fields than

© I.B. Berkutov, V.V. Andrievskii, Yu.F. Komnik, Yu.A. Kolesnichenko, R.J.H. Morris, D.R. Leadley, and O.A. Mironov, 2012

those typical for CR experiment and it is a pure electrical transport measurement. The relative simplicity of SdH experiments is the reason that a majority of effective masses had been measured in this way. In this paper the effective mass of $Si_{1-x}Ge_x$ (x = 0.13, 0.36, 0.95, 0.98) *p*-type QWs have been studied using SdH-technique. From the results a number of deviations from the ideal theoretical model arise, which are associated with structural features of the quantum wells and the technology used to prepare them and will be discussed below.

2. Structure of the samples

All the heterostructures studied here have been designed to have a two-dimensional hole gas (2DHG) in a biaxial compressive strained $Si_{1-x}Ge_x$ alloy channel grown. Three of the heterostructures were grown by the molecular beam epitaxy (MBE) technique and are labelled samples "A", "B", and "C", with quantum wells in $Si_{0.87}Ge_{0.13}$, $Si_{0.64}Ge_{0.36}$, and $Si_{0.05}Ge_{0.95}$ channels, respectively. The detailed MBE growth conditions are as follows. Heterostructure "A" has a 35 nm thick QW of $Si_{0.87}Ge_{0.13}$ grown pseudomorphically at 870 °C on a Si (001) substrate and is remotely doped from above the QW with $2\cdot10^{18}$ cm^{-3} of boron in a 50 nm Si layer grown at 750 °C [6]. Heterostructure "B" is similar with a 10 nm thick pseudomorphic QW of $Si_{0.64}Ge_{0.36}$ grown at 450 °C and annealed *in situ* at 800 °C before completing the structure with remote B-doped above the QW with $2\cdot10^{18}$ cm^{-3} of boron in a 50 nm Si layer grown at 600 °C [7]. Such low-temperature QW growth and *in situ* annealing was used to avoid growth-induced roughening of the top $Si_{0.64}Ge_{0.36}$/Si interface, which was typically observed for growth temperatures above 550 °C and led to dramatically reduced 2DHG mobility in the QW at $T < 10$ K.

Sample "C" was metamorphic, with an intermediate relaxed $Si_{0.4}Ge_{0.6}$ buffer grown on the Si (001) substrate followed by a strained $Si_{0.05}Ge_{0.95}$ QW. In this sample boron doping was introduced both on top and underneath the QW, with similar MBE growth conditions to [8]; however, for sample "C" the doping was asymmetric with the boron-doped $Si_{0.4}Ge_{0.6}$ layers having concentrations of $2\cdot10^{18}$ and $8\cdot10^{18}$ cm^{-3} below and above the QW, respectively.

Metamorphic sample "D" $Si/Si_{0.4}Ge_{0.6}/Si_{0.02}Ge_{0.98}/Si_{0.4}Ge_{0.6}$ was grown using a hybrid-epitaxy technique that used UHV–CVD for the virtual substrate and SS–MBE for the active heterostructure, consisting of a 20 nm $Si_{0.02}Ge_{0.98}$ QW grown at 350 °C with remote/inverted B-doping of $3.6\cdot10^{18}$ cm^{-3} [9]. Sample "D" was also annealed *ex situ* at 650 °C as this had been previously found to yield the highest 2DHG mobility for this type of sample, 22100 cm^2/(V·s) at 10 K. It had been intended that the strained QW for sample "D" was "technologically pure Ge" [9], but characterization after growth and annealing by high resolution XRD and SIMS revealed it to be ~98% Ge [10].

Conventional Hall bar geometries were measured for all the samples. For samples "A", "C", and "D" the diagonal $\rho_{xx}(B)$ and off-diagonal $\rho_{xy}(B)$ components of the resistance tensor were measured up to 11 T whilst for sample "B" it was only measured up to 6 T. The measurements were performed using a standard lock-in technique at a frequency of 33 Hz and a current of 10 nA for samples "A", "B", and "C", with 100 nA used for sample "D". No overheating effects were observed at these current levels. The lowest temperatures of the measurement for the samples were: 33 mK for sample "A", 350 mK for samples "B" and "C", and 1.45 K for sample "D". The measured $\rho_{xx}(B)$ and $\rho_{xy}(B)$ dependencies at these temperatures are shown in Fig. 1 (where $\rho_{xx}(B)$ stands for the resistance per square area of a 2DHG). The curves exhibit pronounced Shubnikov–de Haas oscillations at $B \geq 1$ T and steps representative of the quantum Hall effect plateaux are observed for sample "A". The 2DHG parameters found from the measurement of resistance, Hall effect and Shubnikov–de-Haas oscillations at these temperatures are given in the Table 1.

3. Determination of m^*

The effective mass m^* and quantum scattering time of the charged particles, which leads to the broadening of the Landau levels, are usually estimated from the temperature and magnetic field dependent SdH oscillation amplitude (ΔR). ΔR is the deviation of adjacent maximum and minimum of the resistance from the averaged monotonic resistance R_0 as a function of magnetic field *B*. The change in resistivity (i.e., conductivity) of the 2D gas is a quantum effect and is considered theoretically in Refs. 11, 12. Assuming a homogeneous broadening of the Landau levels, the modulation of the electrical resistance is calculated in Ref. 12 to be:

Table 1. Parameters of 2DHG in strained and remotely doped SiGe QWs

Sample	Quantum channel	ρ_{xx}, kΩ	p_{Hall}, cm^{-2}	p_{SdH}, cm^{-2}	μ_{Hall}, cm^2/(V·s)	m, m_0	α
A	$Si_{0.87}Ge_{0.13}$	3.04	$1.9\cdot10^{11}$	$2.1\cdot10^{11}$	$1.17\cdot10^4$	0.21 ± 0.03	1.02
B	$Si_{0.64}Ge_{0.36}$	4.78	$6.42\cdot10^{11}$	$6.7\cdot10^{11}$	$0.22\cdot10^4$	0.24 ± 0.005	1.05
C	$Si_{0.05}Ge_{0.95}$	0.247	$2.82\cdot10^{12}$	$2.98\cdot10^{12}$	$0.91\cdot10^4$	0.17 ± 0.01	4.4
D	$Si_{0.02}Ge_{0.98}$	0.16	$1.62\cdot10^{12}$	$0.95\cdot10^{12}$	$2.21\cdot10^4$	0.12 ± 0.005	8.6
				$0.68\cdot10^{12}$			20

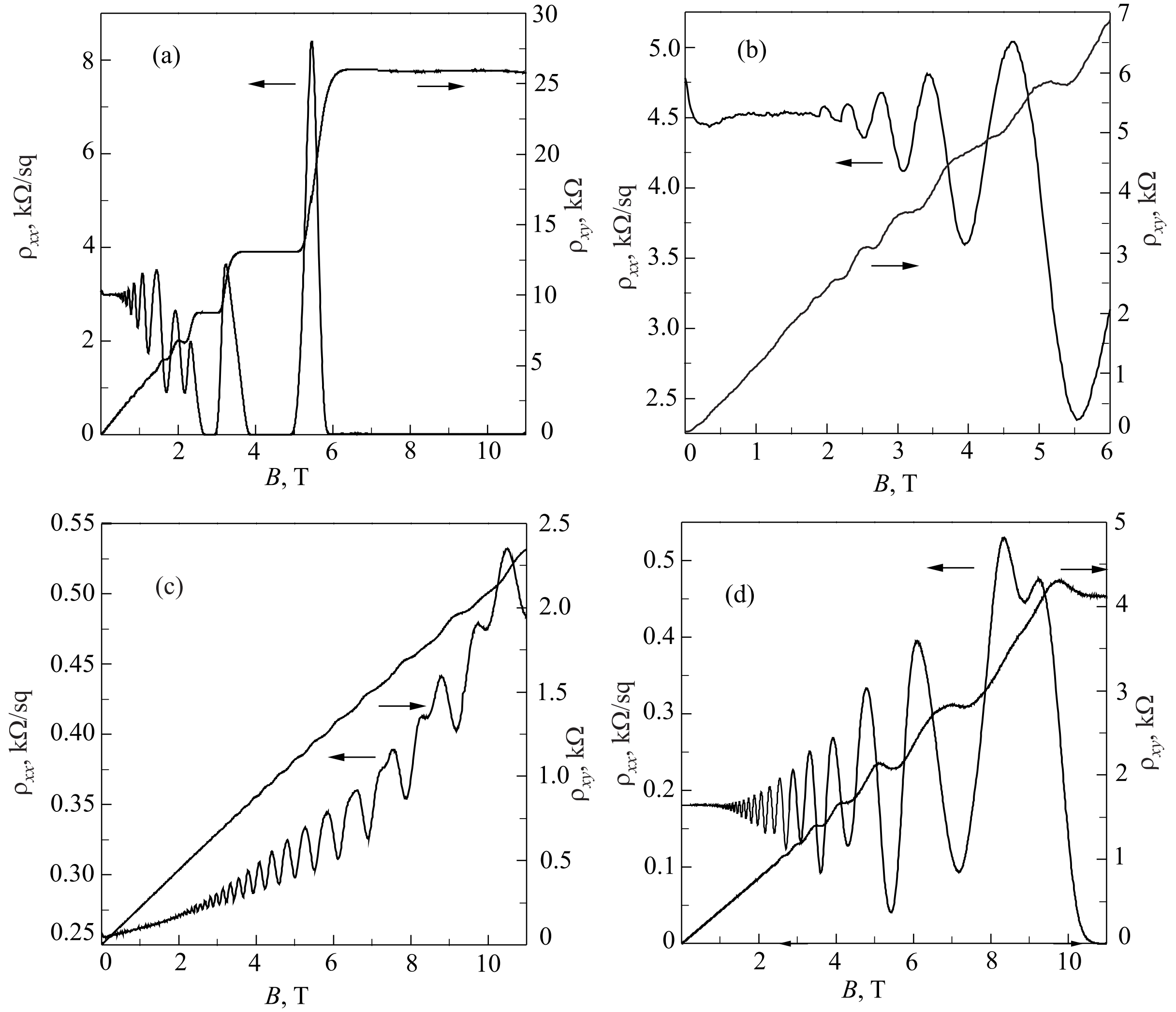

Fig. 1. Magnetoresistance ρ_{xx} and ρ_{xy} of samples "A" (a) at $T = 33$ mK, "B" (b) at 350 mK, "C" (c) at 350 mK, and "D" (d) at $T = 1.45$ K.

$$\rho_{xx}(B) = \rho_0^{-1} \times$$

$$\times \left[1 + 4\sum_{s=1}^{\infty} \left(\frac{\Psi s}{\sinh \Psi s} \right) \exp\left(-\frac{\pi s}{\omega_c \tau_q} \right) \cos\left(\frac{2\pi s \varepsilon_F}{\hbar\omega_c} - s\pi \right) \right], \quad (1)$$

where $\Psi = 2\pi^2 k_B T/(\hbar\omega_c)$ determines the temperature and magnetic field dependencies of the oscillations amplitude and $\omega_c = eB/m^*$ is the cyclotron frequency. The Fermi energy for the 2D case is given by $\varepsilon_F = \pi\hbar^2 n/m^*$, where n is the concentration of charge carriers. In the practice, the term of the summation *s*, in Eq. (1) can be taken to be 1, i.e., $s = 1$ which is correct if $\omega_c \tau_q << 1$ as in a case of investigated samples. The second factor in the summation (called the Dingle factor) describes homogeneous broadening in the Landau levels due to a finite quantum state lifetime τ_q. It should be noted that this lifetime is different [13] from the Drude transport lifetime τ which defines the conductivity $\sigma = ne^2\tau/m^*$. As it follows from our study the value of τ for our samples are almost temperature and magnetic fields independent in investigated temperature and magnetic field range. We assume that value τ_q is also independent of magnetic field and temperature in which case it is not involved in the following analysis. Finally, the first term in the summation describes a damping of the SdH oscillations due to the temperature broadening of the Fermi function.

The mass and concentration of carriers can be found from the period and amplitude of SdH oscillations (at different temperatures) as a function of inverse magnetic field by plotting the dependence $\ln[(\Delta R/R_0)(\sinh\Psi)/\Psi]$ vs $1/(\omega_c\tau)$ or $1/(\mu B)$, where μ is the carrier mobility (Dingle plot). The argument of the exponent term in Eq. (1) can now be rewritten as $-\pi\alpha/(\omega_c\tau)$, $\alpha = \tau/\tau_q$. According to Eq. (1), plotting the points corresponding to the extrema with different numbers ν of Landau levels should result in a straight line with the slope proportional to $\pi\alpha$. In this case the effective mass m^* becomes a fitting parameter [14]. According to the Eq. (1), for an extremely strong magnetic field $(1/\omega_c\tau \to 0)$ $(\sinh\Psi)/\Psi \to 1$ so this straight line should bisect the $\ln[(\Delta R/R_0)(\sinh\Psi)/\Psi]$ axis at a value of $\ln 4 \cong 1.386$. Furthermore, the experimental data for a plot

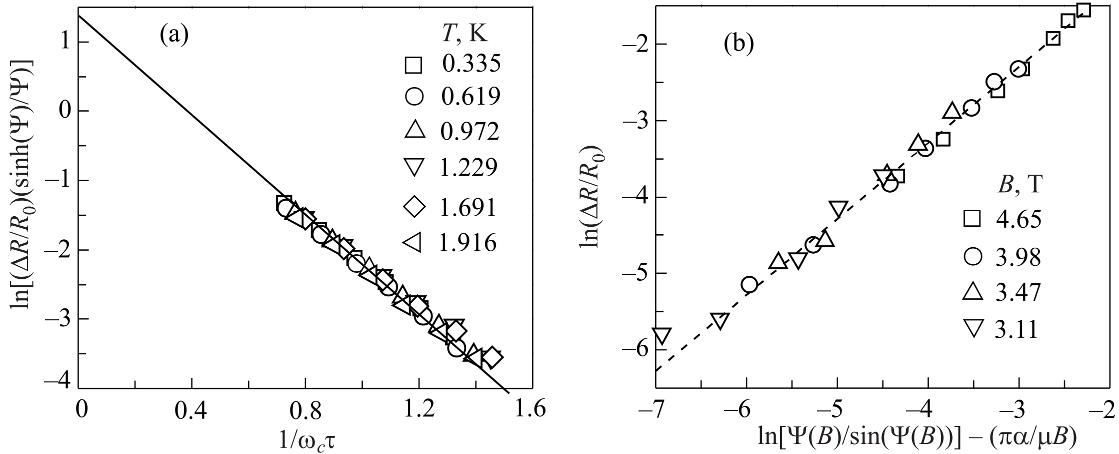

Fig. 2. Plots for self-consistent extraction of effective mass m^* and parameter α for sample "B" for different temperatures (a) and magnetic fields (b).

of $\ln[\Delta R/R_0]$ vs $\ln(\Psi s/\sinh\Psi s)-\pi\alpha/(\omega_c\tau)$, which gives possibility to get value α using it as a fitting parameter, should also result in a straight line with a gradient equal to unity [14].

However, it turns out that the experimental data in many cases could not be exactly fitted by a single straight line for all magnetic fields, but instead shows a curve, deviations at small values of the arguments and/or different intercept values.

An example of the method described above for the determination of m^* is presented in Fig. 2 for sample "B". From this analysis m^* was estimated to be $0.24\,m_0$ (where m_0 is free electron mass) and $\alpha = 1.05$. The solid line on Fig. 2 is the straight line predicted by Eq. (1) with an intercept at ln 4 which fits well to the experimental data. Figures 3–5 show similar analysis for the other samples that illustrate a number of deviations from the dependence predicted by Eq. (1), both quantitatively and qualitatively, that are typical of the deviations seen in many previous reports. In the discussion below, we will show how these deviations can be associated with structural features of the QWs and the technology used in their preparation.

4. Deviations from the theory

4.1. Influence of Zeeman spin splitting

Looking at the Dingle plot in Fig. 2(a) for sample "B", the data from weak magnetic fields in the limit $1/\omega_c\tau \to 0$ follows the straight line that intercepts at $\ln 4$. However, for strong magnetic fields $(1/\omega_c\tau < 1.3)$ a small deviation downward is observed. This is because the amplitude of the SdH oscillations is less than expected in the theory, due to spin (Zeeman) splitting affecting the maxima and changes in the SdH oscillation shape as the resistivity approaches zero in the minima (see Fig. 1(a)). In the limit of strong magnetic fields the spin splitting obviously splits the SdH oscillations maxima and such extreme are clearly not included in the m^* calculation; however, for intermediate magnetic fields the spin splitting may not be fully resolved, but still result in a decrease of the observed the oscillation amplitude and leads to a deviation from the theory [12].

4.2. Extra "inhomogeneous broadening" of the Landau levels

Attention has previously been drawn to the nonlinearity in the $\ln[(\Delta R/R_0)(\sinh\Psi)/\Psi]$ vs $1/(\omega_c\tau)$ dependence in high-mobility systems, for instance in [15,16]. For low magnetic fields the reason for the deviation from the theory is as follows: it is assumed [16] that in some cases (mainly in high-mobility systems with a 2D gas of charge carriers) the nonlinearity appears because of a spatial change (in the 2D gas plane) of the electron concentration and hence in the Fermi energy. As the result, the oscillation extrema in different parts of the sample occur at slightly different magnetic fields and so the total oscillation amplitude decreases in comparison with its value from a homogeneous sample. This leads to an additional effective broadening of the Landau levels (so-called "inhomogeneous broadening") [16].

The formation of the SdH oscillations in the case of long-range fluctuations (i.e., in the plane of 2D gas) in of the potential, electron concentration, and Fermi energy are described by a Gaussian in Ref. 16. It was shown that an additional term $-[\pi\delta\varepsilon_F/(\hbar\omega_c)]^2$ does appears in the argument of the exponential describing the oscillation amplitude in Eq. (1). The exponential factor in Eq. (1) therefore becomes

$$\exp\left[-\frac{\pi}{\omega_c\tau_q}-\left(\frac{\pi^2\hbar\delta n}{m^*\omega_c}\right)^2\right]. \qquad (2)$$

The first term in the exponent still describes the collision's broadening of the Landau levels and is inversely proportional to the magnetic field. The second term now accounts

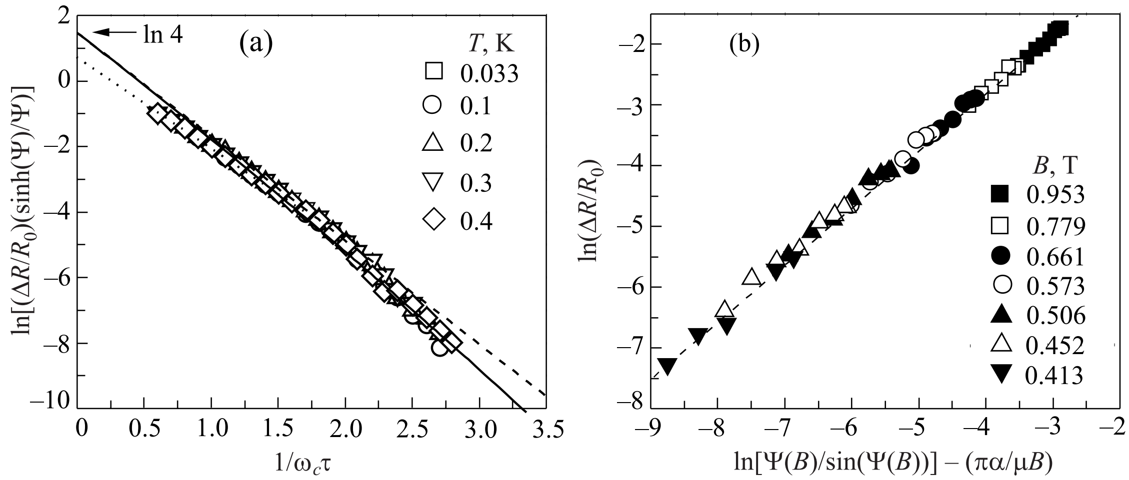

Fig. 3. Plots for self-consistent extraction of effective mass m^* and parameter α for sample "A" for different temperatures (a) (solid line is theory [12]) and magnetic fields (b). The dashed line is guides to the eye.

for the "inhomogeneous broadening" of the Landau levels and is inversely proportional to the square of the field.

Figure 3(a) illustrates the possibility of describing the experimental dependencies $Y = \ln\,[(\Delta R/R_0)(\sinh\Psi)/\Psi]$ vs $X = 1/(\omega_c\tau)$ by the polynomial $Y = -a_1 X - a_2 X^2 + \text{const}$ where according to Eqs. (1) and (2), $a_1 = \pi\tau/\tau_q$ and $a_2 = (\pi^2\hbar\tau\delta p/m^*)^2$. From this approximation $m^* = (0.21 \pm 0.03)m_0$ and $\alpha = 1.02$ are found using the linear term (dashed line in Fig. 3(a)), and $\delta p = 4\cdot 10^9$ cm^{-2} from the quadratic term [17] which is only 2% of the $p_{SdH} = 2.1\cdot 10^{11}\,\text{cm}^{-2}$.

4.3. The large positive quasiclassical magnetoresistance

For sample "C" the above described procedure when the resistance in zero field ($\rho_0 \sim 1/\sigma_0$) was applied. The Dingle plot for all the experimental points results in a straight line (open symbol in Fig. 4(a)). However, extrapolation of this line to $1/\omega_c\tau \to 0$ (dashed line in Fig. 4(a)) does not give the value $\ln 4$. The reason for this discrepancy with Eq. (1) is the presence of a large positive change in the monotonic background of the magnetoresistance (see Fig. 1(c)). This positive change is well described by the function $\rho_{xx}(B)/\rho_{xx}(0) \propto B^{12/7}$ as predicted by quasiclassical theory [18,19], which considered the combined influence of a short-range potential from the scattering centers in the quantum channel and the long-range potential from impurity atoms in the remote doping layers. This monotonic background results in the deviation of resistance values at the minima and maxima in the SdH oscillations does not result from a constant ρ_0, but from the values $\rho_B = \rho_0 + \Delta\rho(B)$ which are determined by the change of the monotonic background of the magnetoresistance. To take into account this monotonic background, the calculations according to Eq. (1) were carried out using ρ_B instead of ρ_0. Therefore, the dependence $\ln\,[(\Delta R/R_0)(\sinh\Psi)/\Psi] + \ln[\rho_B(B)/\rho_0]$ vs $1/(\mu B)$ (up to a constant term) should be used instead of dependence

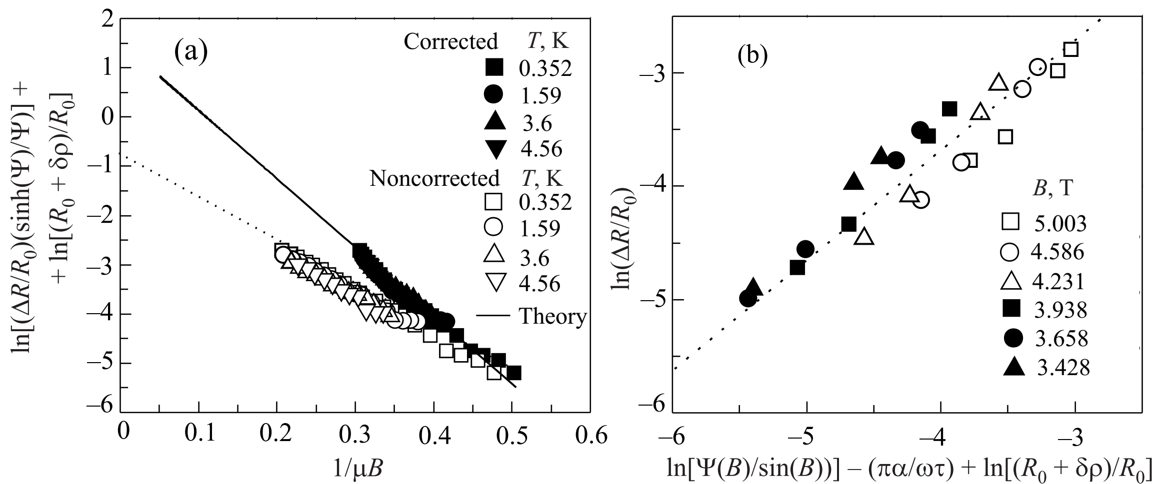

Fig. 4. Plots for self-consistent extraction of effective mass m^* and parameter α for sample "C" for different temperatures (a) (open symbols is calculation with $\sigma_0^{-1} = \rho_0(B = 0)$, dark symbols is calculation with taking into account the magnetic field dependence of the monotonous background of magnetoresistance) and magnetic fields (b). The dashed line is guides to the eye.

$\ln[(\Delta R/R_0)(\sinh\Psi)/\Psi]$ vs $1/(\mu B)$ to obtain the abscissa in Fig. 4(a). The dark symbols in Fig. 4(a) show the experimental points obtained while the solid line demonstrates the theory given in [12] and yields value of $\ln 4$ at $1/(\omega_c\tau)\to 0$. Based on this appropriate adjustments were made for the calculations made on the curves of Fig. 4(b). The estimate for the effective mass of the sample "C" is $m^* = 0.17m_0$, whereas $\alpha = 4.4$.

4.4. 2D systems with two populated subbands

The results from the calculations for sample "D" which were done according to the theory [12] are shown in Fig. 5. It

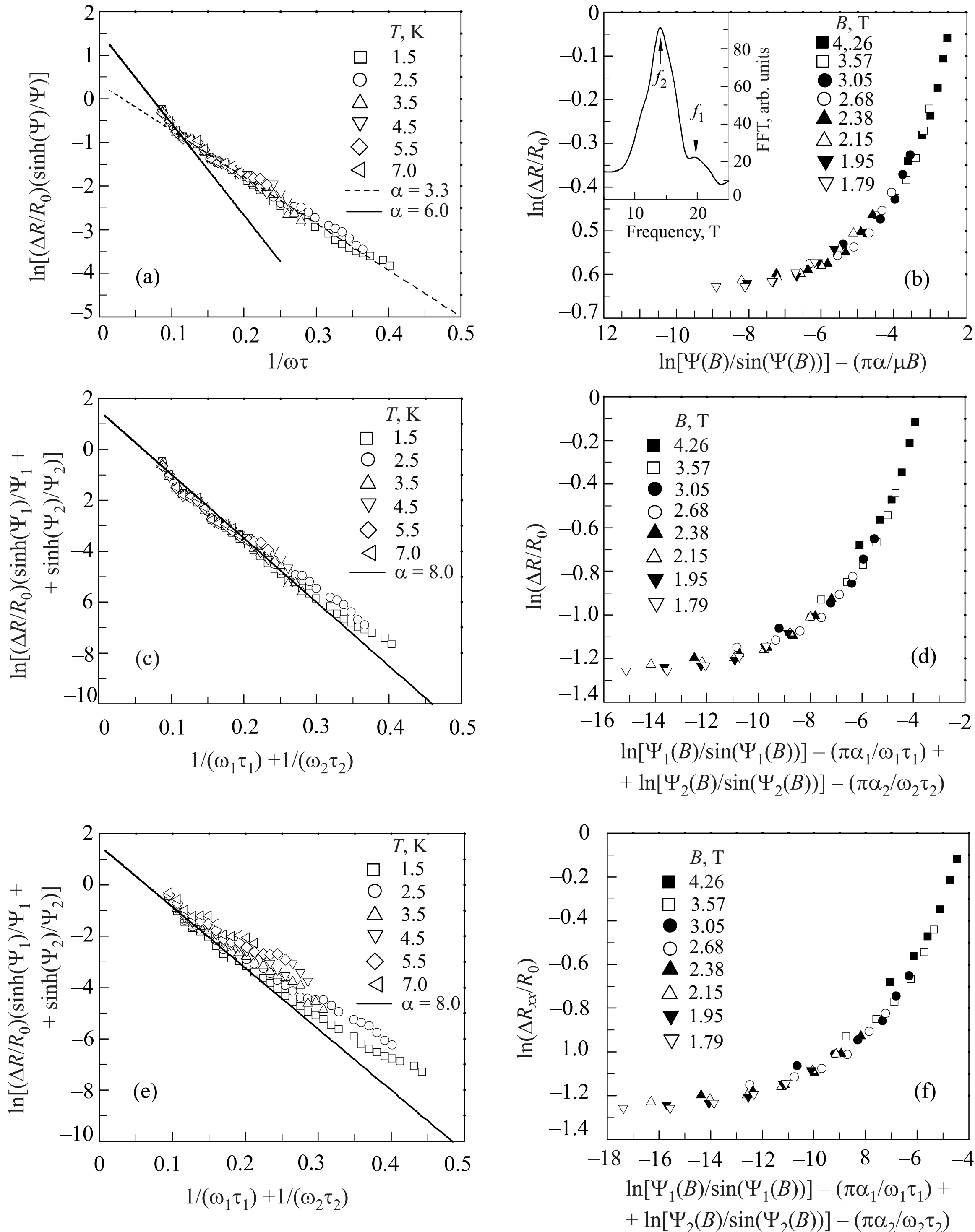

Fig. 5. Plots for self-consistent extraction of effective mass m^* and parameter α for sample "D" for different temperatures and magnetic fields using theoretical model [12] for $m^* = 0.12m_0$ (a) and $\alpha = 8$ (b); with existence of two levels of magnetic quantization taken into account for $m_1^* = m_2^* = 0.12m_0$ (c), $\alpha_1 = 8.6$, $\alpha_2 = 20$ (d) and $m_1^* = 0.12m_0$, $m_2^* = 0.147m_0$ (e), $\alpha_1 = 6.4$, $\alpha_2 = 24$ (f) calculated according to theory [21]. Inset: FFT of SdH oscillation at $T = 1.45$ K showing two periods.

is seen (Fig. 5(a)) that the experimental curve is considerably nonlinear and has a kink at $B \sim 3.5$ T, while at the same point a single curve in Fig. 5(a) can be obtained with at a value of m^* equals $m^* = 0.12\,m_0$. However, two values of α are found. For strong magnetic fields, i.e., before the kink in Fig. 5(a) a value of $\alpha = 3.3$ is found. At lower magnetic fields this value is approximately $\alpha = 6$. The experimental curve in Fig. 5(b) is also considerably nonlinear, but the experimental points for the various magnetic fields can be arranged on a single curve by using a value $\alpha = 8$. Fast Fourier transform analysis of the oscillatory part of $\rho_{xx}(B)$ (see inset in Fig. 5(b)) revealed the presence of two maxima. From the data combined with the effect of "beating" observed in the SdH oscillations (see Fig. 1(d)) we conclude that two populated hole subbands exist, hence the two sets of SdH oscillations. The frequencies $f_1 = 19.5$ T and $f_2 = 14$ T are found and correspond to the first and second subbands with a hole concentration $p_1 = 2ef_1/h = 0{,}95\cdot 10^{12}$ cm^{-2} and $p_2 = 2ef_2/h = 0.68\cdot 10^{12}$ cm^{-2}, respectively. The same time, the sum of these values, i.e., $p_1 + p_2$, yields a similar concentration to that obtained from Hall measurements to within 1 %. Thus, we conclude that a simple theoretical model [12] is in applicable in this case. Early models that describe the magnetoresistance of 2D systems in the presence of two populated subbands [20,21] do not give a successful description of experimental results and theory [21] is in applicable here because the magnetic quantized subbands are not completely filled. The most successful description of our data is obtained by using the theoretical model [23,24], where the resistance of the 2D system is represented as [24]

$$\rho = \rho^{(0)} + \rho^{(1)} + \rho^{(2)}, \tag{3}$$

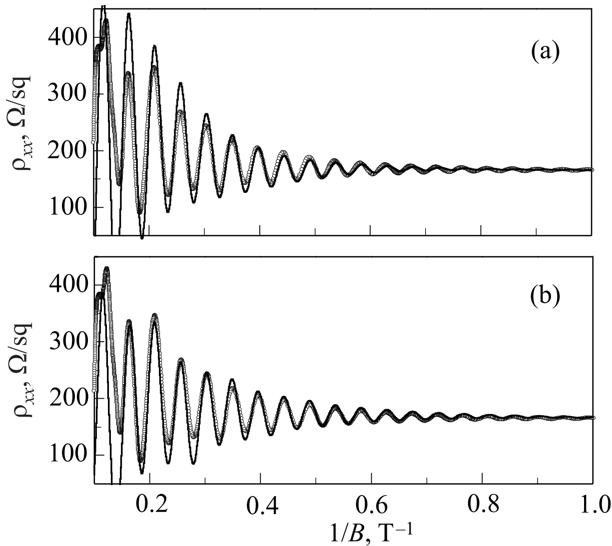

Fig. 6. Dependence of magnetoresistance ρ_{xx} of sample "D" on inverse magnetic field (open symbols). The solid line is due to the theory [23,24] for the cases when $m_1^* = m_2^* = 0.12m_0$ (a) and $m_1^* = 0.12m_0$, $m_2^* = 0.147m_0$ (b).

where $\rho^{(0)}$ is the classical resistance, $\rho^{(1)}$ is the first-order quantum correction describing the SdH oscillations, $\rho^{(2)}$ is the second-order quantum contribution. The classical resistance is

$$\rho^{(0)} = \frac{m^*}{e^2 p_s}\,\frac{\omega_c^2 v_s + v_0 v_r^2}{\omega_c^2 + v_r^2}. \tag{4}$$

Here $p_s = p_1 + p_2$ is total density of charge carriers, ω_c is cyclotron frequency, The characteristic rates v_s, v_r, and v_0 are given by

$$v_s = \left(\frac{p_1}{p_s}\right) v_{11}^{\text{tr}} + \left(\frac{p_2}{p_s}\right) v_{22}^{\text{tr}} + v_{12}^{\text{tr}},$$

$$v_r = \left(\frac{p_2}{p_s}\right) v_{11}^{\text{tr}} + \left(\frac{p_1}{p_s}\right) v_{22}^{\text{tr}} + 2v_{12} - v_{12}^{\text{tr}},$$

$$v_0 = \frac{D}{\nu_r},\quad D = (v_{11}^{\text{tr}} + v_{12})(v_{22}^{\text{tr}} + v_{12}) - \frac{(v_{12} - v_{12}^{\text{tr}})^2\, p_s^2}{4 p_1 p_2},$$

where v_{ij} are the elastic quantum scattering rates in the absence of magnetic field, v_{ij}^{tr} are transport rates for intrasubband scattering. The first-order quantum contribution is [24]

$$\rho^{(1)} = -I\frac{2m^*}{e^2 p_s}\sum_{j=1,2}\left[\frac{2p_j}{p_s} v_{jj}^{\text{tr}} + v_{12}^{\text{tr}}\right]\exp(-\alpha_j)\cos\frac{2\pi(\varepsilon_F - \varepsilon_j)}{\hbar\omega_c}, \tag{5}$$

where $\alpha_j = \pi v_j/\omega_c$, $v_j = v_{jj} + v_{12}$, ε_j is subband energies, $I = \Psi/\sinh\Psi$ with $\Psi = 2\pi^2 T/\hbar\omega_c$. The second-order quantum contribution which describes both the positive magnetoresistance and the magnetointersubband (MIS) oscillations [25], whose maxima correspond to integer ratios of the subband splitting energy $\Delta_{12} = \varepsilon_2 - \varepsilon_1$ to the cyclotron energy $\hbar\omega_c$ [24] is given by

$$\rho^{(2)} = \frac{2m^*}{e^2 p_s}\left[\frac{p_1}{p_s} v_{11}^{\text{tr}} e^{-2\alpha_1} + \frac{p_2}{p_s} v_{22}^{\text{tr}} e^{-2\alpha_2} + v_{12}^{\text{tr}} e^{-\alpha_1 - \alpha_2}\cos\frac{2\pi\Delta_{12}}{\hbar\omega_c}\right]. \tag{6}$$

The results obtained by using the models given in [23,24] are shown in Fig. 6(a). The following kinetic characteristics of the sample were obtained: the effective mass $m^* = 0.12m_0$; while the values of parameter α at each subband are $\alpha_1 = 8.6$ and $\alpha_2 = 20$; and $\Delta_{12} = 18.7$ meV; $\nu_{12} = 4\cdot 10^{11}$ s^{-1}. A simple account of existence of the two subbands in the constructions analogous to those for other samples (see Figs. 5(c) and 5(d)) showed that the experimental points form a monotonic curve when found, according to the theory [23,24], parameters are used (this constric-

tion do not include the second-order quantum contribution and is applicable in the case when the last is small).

It was shown [10] that for a similar structure to that of the sample "D" the two different values of the effective mass $m_1^* = 0.12m_0$ and $m_2^* = 0.147m_0$ could be expected based on the 4×4 Luttinger Hamiltonian calculations (for simplified case of rectangular QW). At low magnetic fields $B \sim 5$ T only one broad CR line was observed with an effective cyclotron mass of $m_1^* = 0.12m_0$, which coincides with calculated CR effective mass in the first electric subband. The width of CR line had been explained by CR transitions from these two subbands at different fields which results insignificant CR line significant broadening [10]. The two different values of m^* were also reported in Ref. 26 where it was shown that the lowest hole bound state in the surface potential well at the GaAs–(AlGa)As heterojunction interface consists of two subbands, and are degenerate at $k = 0$. The lifting of the spin degeneracy at $k \neq 0$, due to the lack of inversion symmetry at the heterojunction interface, gives rise to two cyclotron masses: $m_1^* = 0.36m_0$ and $m_2^* = 0.6m_0$.

This possibility was further explored by using the above values of the effective mass. The results from experimental studies of the inverse magnetic field dependence of the resistance in the framework of the theory [23,24] are shown in Fig. 6(b). Comparison of the results presented in Fig. 6(a) and 6(b) and does not appear to show any significant difference. At the same time a simple account of existence of the two different values of m^* on different subbands (see Fig. 5(e) and 5(f)) showed that the experimental points are not form a single monotonic curve.

For more precise statement the additional study using the cyclotron resonance method is necessary.

5. Conclusion

In this work the 2DHG effective mass m^* for a number of different Ge concentration in SiGe QW structures has been determinates from Shubnikov–de Haas oscillations. It has been shown that the deviation of our experimental data from theory [12] as described by the SdH-related conductivity oscillations may be explained by the following:

— Spin splitting of the SdH oscillations maxima, which results in a decrease in the oscillations amplitudes;

— Extra broadening of the Landau levels which is attributed to the existence of a 2% inhomogeneous distribution in the carrier concentration of the 2D charge layer and, hence, their energy. It is believed that the extra broadening is from the natural variation of well width that is of interatomic distance scale [16];

— Observation of both SdH oscillations and the nonsaturating large positive quasiclassical magnetoresistance which is a consequence of the short and long-range scattering potentials as predicted by the theory [18].

In the case when more than one quantized subband is filled the analysis of SdH oscillations according the simple model given in [12] becomes unusable. In this case, a more detailed analysis is necessary.

Acknowledgments

The authors thank to T. Hackbarth (Daimler AG Forschungszentrum, 89081 Ulm, Germany), for the MBE growth/fabrication of the sample "C". Measurements were made at the Nanosilicon Group, Department of Physics, University of Warwick, Coventry, UK, and partially at the International Laboratory of High Magnetic Fields and Low Temperatures, Wroclaw, Poland.

1. B. Rössner, D. Chrastina, G. Isella, and H. von Känel, *Appl. Phys. Lett.* **84**, 3058 (2004).
2. M. Myronov, K. Sawano, Y. Shiraki, T. Mouri and K.M. Itoh, *Appl. Phys. Lett*. **91**, 082108 (2007).
3. J.B. Roldán and F.Gámiz, *Solid-State Electron*. **48**, 1347 (2004).
4. I.M. Lifshits, *Zh. Exp. Teor. Fiz.* **40**, 1235 (1961).
5. S.M. Sze, *Phys. Semicond. Devices*, New York, Wiley (1981).
6. T.E. Whall, D.W. Smith, A.D. Plews, R.A. Kubiak, P.J. Phillips, and E.H.C. Parker, *Semicond. Sci. Technol* **8**, 615 (1993).
7. T.J. Grasby, C.P. Parry, P.J. Phillips, B.M. McGregor, R.J.H. Morris, G. Braithwaite, T.E. Whall, E.H.C. Parker, R. Hammond, A.P. Knights, and P.G. Coleman, *Appl. Phys. Lett*. **74**, 1848 (1999).
8. G. Höck, M. Glück, T. Hackbarth, H.J. Herzog, and E. Kohn, *Thin Solid Films* **336**, 141 (1998).
9. R.J.H. Morris, T.J. Grasby, R. Hammond, M. Myronov, O.A. Mironov, D.R. Leadley, T.E. Whall, E.H.C. Parker, M.T. Currie, C.W. Leitz, and E.A. Fitzgerald, *Semicond. Sci. Technol* **19**, L106 (2004).
10. O.A. Mironov, M. Goiran, J. Galibert, D.V. Kozlov, A.V. Ikonnikov, K.E. Spirin, V.I. Gavrilenko, G. Isella, M. Kummer, H. von Känel, O. Drachenko, M. Helm, J. Wosnitza, R.J.H. Morris, and D.R. Leadley, *J. Low Temp. Phys.* **159**, 216 (2010).
11. T. Ando, *J. Phys. Soc. Jpn.* **37**, 1233 (1974).
12. A. Isihara and L. Smrčka, *J. Phys. C* **19**, 6777 (1986).
13. P.T. Coleridge, R. Stoner, and R. Fletcher, *Phys. Rev. B* **39**, 1120 (1989).
14. T.E. Whall, N.L. Mattey, A.D. Plews, P.J. Phillips, O.A. Mironov, R.J. Nicholas, and M.J. Kearney, *Appl. Phys. Lett.* **64**, 357 (1994); T.E. Whall, A.D. Plews, N.L. Mattey, and E.H.C. Parker, *Appl. Phys. Lett*. **65**, 3362 (1994).
15. J.P. Harring, R.J. Higgins, R.K. Goodall, P.R. Lay, M. Laviron, and P. Delesduse, *Phys. Rev. B* **32**, 8126 (1985).
16. S.D. Bystrov, A.M. Kreshchuk, Le Tuan, S.V. Novikov, T.A. Polyanskaya, I.G. Saveliev, and A.Ya. Shik, *Fiz. Tehn. Poluprovod*. **28**, 91 (1994).

17. I.B. Berkutov, V.V. Andrievskii, Yu.F. Komnik, O.A. Mironov, M. Myronov, and D.R. Leadley, *Fiz. Nizk. Temp*. **35**, 188 (2009) [*Low Temp. Phys*. **35**, 141 (2009)].
18. D.G. Polyakov, F. Evers, and P. Wölfle, *Phys. Rev. B* **64**, 205306 (2004).
19. I.B. Berkutov, V.V. Andrievskii, Yu.F. Komnik, and O.A. Mironov, *Fiz. Nizk. Temp*. **36**, 1335 (2010) [*Low Temp. Phys*. **36**, 1076 (2010)].
20. D.R. Leadley, R. Fletcher, R.J. Nicholas, F. Tao, C.T. Foxon, and J.J. Harris, *Phys. Rev. B* **46**, 12439 (1992).
21. T.H. Sander, S.N. Holmes, J.J. Harris, D.K. Maude, and J.C. Portal, *Phys. Rev. B* **58**, 13856 (1998).
22. M.E. Raikh and T.V. Shahbazyan, *Phys. Rev. B* **49**, 5531 (1994).
23. O.E. Raichev, *Phys. Rev. B* **78**, 125304 (2008).
24. N.C. Mamami, G.M. Gusev, E.C.F. da Silva, O.E. Raichev, A.A. Quivy, and A.K. Bakarov, *Phys. Rev. B* **80**, 085304 (2009).
25. N.C. Mamani, G.M. Gusev, T.E. Lamas, A.K. Bakarov, and O.E. Raichev, *Phys. Rev. B* **77**, 205327 (2008).
26. H.L. Stormer, Z. Schlesinger, A. Chang, D.C. Tsui, A.C. Gossard, and W. Wiegmann, *Phys. Rev. Lett*. **51**, 126 (1983).